Ultra-short dual-core GaAs photonic crystal fiber splitter filled with nematic liquid crystal

Sinuo An,[a] Ying Shi,[b,c] Zao Yi,[d] Chao Liu,[a,*] Tao Sun,[e] Jingwei Lv,[a] Lin Yang,[a] and Paul K. Chu[f,g,h]

[a]Northeast Petroleum University, School of Physics and Electronic Engineering, Daqing, China
[b]Northeast Petroleum University, Institute of Unconventional Oil and Gas, Daqing, China
[c]The Fourth Affiliated Hospital of Harbin Medical University, Department of Gynecology and Obstetrics, Harbin, China
[d]Southwest University of Science and Technology, Joint Laboratory for Extreme Conditions Matter Properties, Mianyang, China
[e]Massachusetts Institute of Technology, Media Lab, Cambridge, Massachusetts, United States
[f]City University of Hong Kong, Department of Physics, Tat Chee Avenue, Kowloon, Hong Kong, China
[g]City University of Hong Kong, Department of Materials Science and Engineering, Tat Chee Avenue, Kowloon, Hong Kong, China
[h]City University of Hong Kong, Department of Biomedical Engineering, Tat Chee Avenue, Kowloon, Hong Kong, China

Abstract. A simple nematic liquid crystal-filled dual-core photonic crystal fiber polarization beam splitter is designed and analyzed by the full-vector finite element method. The length of the polarization beam splitter is 13.3390 μm and the maximum extinction ratio (ER) is 143.49 dB. The bandwidth of ERs greater than 10 dB is 200 nm at a wavelength of 1.55 μm. This simple and easy-to-manufacture structure has great potential in miniaturized communication devices. © *2021 Society of Photo-Optical Instrumentation Engineers (SPIE)* [DOI: 10.1117/1.OE.60.5.056104]

Keywords: optical crystal fibers; polarization beam splitter; coupling length; extinction ratio.

Paper 20201426 received Dec. 4, 2020; accepted for publication May 4, 2021; published online May 21, 2021.

1 Introduction

A dual-core fiber contains a pair of parallel cores exploiting coupling of the evanescent field between the two cores to carry out specific optical functions. Compared with the conventional optical fiber composed of a core and cladding, the twin-core optical fiber has a special structure rendering it useful not only as an optical transmission medium but also in new optical waveguide devices, such as polarization splitters,[1–3] coherent detectors,[4] wavelength division multiplexers,[5] optical switches, and filters.[6,7] Recently, the photonic crystal fiber (PCF)[8–10] has attracted much attention because of its flexible structure, which provides the possibility of designing dual-core fibers and new fiber polarization beam splitters.

The birefringence effect caused by the asymmetry of the dual-core PCF structure yields different coupling lengths and allows separation of different polarization states. In 2003, Zhang and Yang[11] reported a 1.7-mm-long polarization splitter based on dual-core PCFs with extinction ratio (ER) of 11 dB and bandwidth of 40 nm. Since then, polarization beam splitters based on dual-core PCFs have been developed. In 2016, Yong et al.[12] proposed an octagonal dual-core PCF polarization splitter with a bandwidth of 37 nm and splitting ratio of 81.2 dB at 1550 nm. In 2019, Fahmi et al.[13] designed a dual-core splitter with a coupling length of 132 m and bandwidth of 301 nm. Recently, Úsuga-Restrepo et al.[14] described an all-fiber circular polarization beam splitter with a length of 24.76 mm, ER of 50 dB, and bandwidth of 36.79 nm (ER > 20 dB).

*Address all correspondence to Chao Liu, msm-liu@126.com

In general, these beam splitters have a wide bandwidth, large ER, or short length, but none of them can satisfy the requirement of a wide bandwidth, high ER, and short length at the same time.

Herein, a simple "nematic liquid crystal" (NLC)-filled PCF polarization splitter is designed. To enhance the asymmetry of the structure, two circular pores filled with NLC are introduced to the vertical axis in the center, consequently increasing the coupling length of the beam splitter. The full-vector finite element method[15–18] is implemented to analyze the PCF polarization filter. A polarization beam splitter with a length of 13.339 μm, ER of 143.49 dB, and bandwidth of 200 nm (for ER $>$ 10 dB) is achieved at 1550 nm. In addition to these excellent properties, this polarization beam splitter has a simple structure that is easy to manufacture and a performance that can be further improved by optimizing the diameter of each hole.

2 Model and Method

The cross section of the dual-core PCF polarization beam splitter is depicted in Fig. 1 in which the white areas are the air holes with diameters of d_0 and d_1 and air hole spacing of Λ. The two central air holes in the optical fiber are circular and have a diameter of d_2. Therefore, two cores denoted by A and B are formed. The gray area is the base material of the optical fiber, that is, gallium arsenide (GaAs). The refractive index is obtained by the following formula:

$$n_{\mathrm{GaAs}}(\lambda) = \sqrt{A_1 + \frac{B_1\lambda^2}{\lambda^2 - \lambda_1^2} + \frac{D\lambda^2}{\lambda^2 - \lambda_2^2} + \frac{F\lambda^2}{\lambda^2 - \lambda_3^2}}, \tag{1}$$

where $A_1 = 5.372514$, $B_1 = 5.466742\ \mu\mathrm{m}^2$, $\lambda_1 = 0.4431307\ \mu$m, $D = 0.2429960\ \mu\mathrm{m}^2$, $\lambda_2 = 0.8746453\ \mu$m, $F = 1.957522\ \mu\mathrm{m}^2$, and $\lambda_3 = 36.9166\ \mu$m. At a wavelength of 1.55 μm, the refractive index of GaAs is 2.03. Figure 1 shows the cross section of the splitter with center holes infiltrated with NLC of type E7. The permittivity tensor of the E7 material has the diagonal form $[{n_e}^2, {n_o}^2, {n_o}^2]$. The anisotropic NLC materials have two refractive indices, the ordinary index (n_o) and the extraordinary index (n_e), which are calculated by the following Cauchy formula:[19–21]

$$n_{o(e)}(\lambda) = A_{o(e)} + \frac{B_{o(e)}}{\lambda^2} + \frac{C_{o(e)}}{\lambda^4}, \tag{2}$$

where λ is the incident wavelength and A_o, B_o, C_o, A_e, B_e, and C_e are the coefficients of the Cauch model, where $A_o = 1.6933$, $B_o = 0.0070\ \mu\mathrm{m}^2$, $C_o = 0.0004\ \mu\mathrm{m}^4$, $A_e = 1.6933$, $B_e = 0.0078\ \mu\mathrm{m}^2$, and $C_e = 0.0028\ \mu\mathrm{m}^4$.

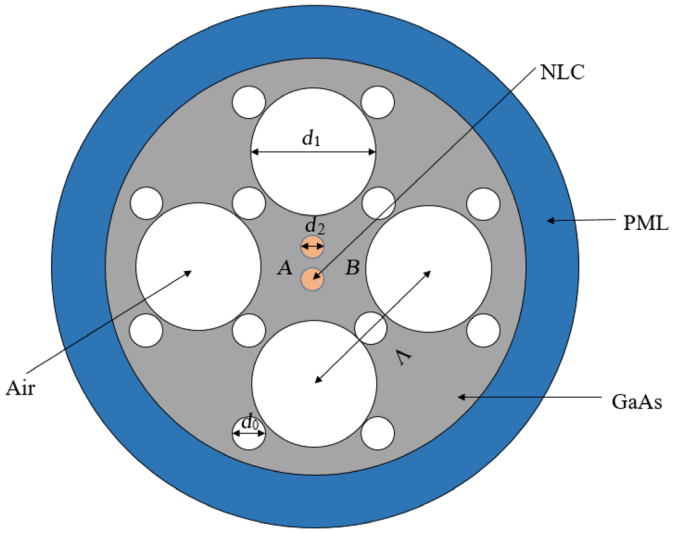

Fig. 1 Cross-sectional structure of the beam splitter.

According to the coupled-mode theory, there are four field distributions in the fiber model, namely the odd and even modes of the x-polarization and y-polarization states. The coupling length is[22]

$$L_{x(y)}^{\lambda} = \frac{\lambda}{2(n_{x(y)}^{e} - n_{x(y)}^{o})}, \tag{3}$$

where $n_{x(y)}^{e}$ is the real part of the effective refractive index of the even mode in the x-polarized and y-polarized directions, respectively, and $n_{x(y)}^{o}$ is the real part of the effective refractive index of the odd modes in the x-polarized and y-polarized directions, respectively. When the coupling length of the polarization beam splitter satisfies $L = L_x/L_y = 0.5$, the x-polarization and y-polarization in the two cores can be separated completely. The confinement loss of the fiber of this mode can be obtained from the imaginary part of the effective refractive index n_{eff} of the mode. The relationship between the confinement loss and wavelength of each mode is[23,24]

$$L = 8.686 \times \frac{2\pi}{\lambda} \operatorname{Im}(n_{\text{eff}}) \times 10^{6}. \tag{4}$$

The relationship between the x-polarization and y-polarization output power and input power of the polarization beam splitter is expressed as[25]

$$P_{\text{out}}^{x,y} = P_{\text{in}}^{x,y} \cos^2\left(\frac{\pi}{2} \cdot \frac{L}{L_c^{x,y}}\right), \tag{5}$$

where L is the transmission distance. The ER is an index that measures the stability of polarization-dependent devices to maintain the polarization state. When a beam of polarized light is incident precisely along a certain optical axis of the polarization-maintaining device, the polarization mode will be excited in the direction of the orthogonal axis. The power ratio of the two orthogonal axes is the extinction ratio of the light source, referred to as the "ER." The ER is expressed as[26]

$$\text{ER} = 10 \log_{10}\left(\frac{P_{\text{out}}^{x}}{P_{\text{out}}^{y}}\right), \tag{6}$$

where P_{out}^{x} and P_{out}^{y} represent the output power of x-polarization and y-polarization, respectively.

3 Results and Discussion

Figure 2 shows the dispersion curve and loss spectra. As the wavelength increases, the effective refractive indices of the four supermodes decrease and losses increase, although the overall loss is still very small.

While keeping the other parameters unchanged, the relationship between Λ (changing from 1.2 to 1.8 μm in steps of 0.1 μm) and the coupling length is shown in Fig. 3. The coupling lengths in the x-polarized and y-polarized directions increase nonlinearly with air hole pitches (Λ) at 1.55 μm. As Λ increases, the distance between the two cores increases. At the same time, the coupling length of the polarization beam splitter increases and the coupling effect decreases. However, Λ cannot be reduced indefinitely, which increases the difficulty in production. By considering all of the factors, the optimal value of Λ is 1.2 μm. Similarly, while keeping the other parameters unchanged, when d_0 is changed from 0.21 to 0.26 μm in steps of 0.01 μm, the relationship between the coupling length and coupling length ratio (CLR) is shown in Fig. 4. The coupling lengths in both the x and y directions diminish as d_0 increases, and when $d_0 = 0.251$ μm, CLR is 0.5.

Figure 5 shows the coupling length in the x-polarization and y-polarization directions and CLR for different apertures of d_1. As the wavelength increases, the coupling lengths for both x and y decrease, and when $d_1 = 1.4$ μm, CLR is 0.5.

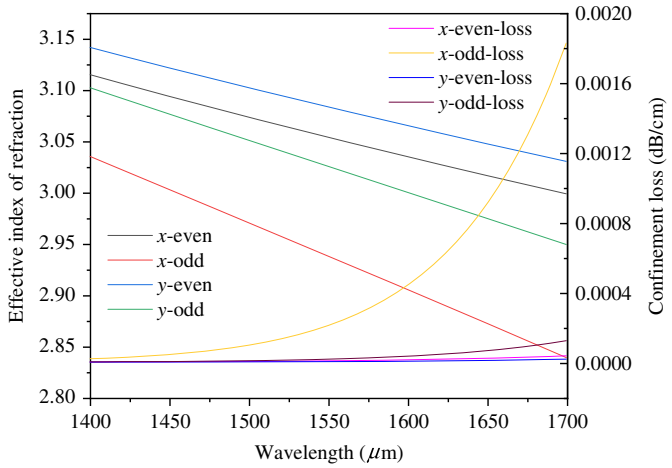

Fig. 2 Dispersion curve and loss spectra.

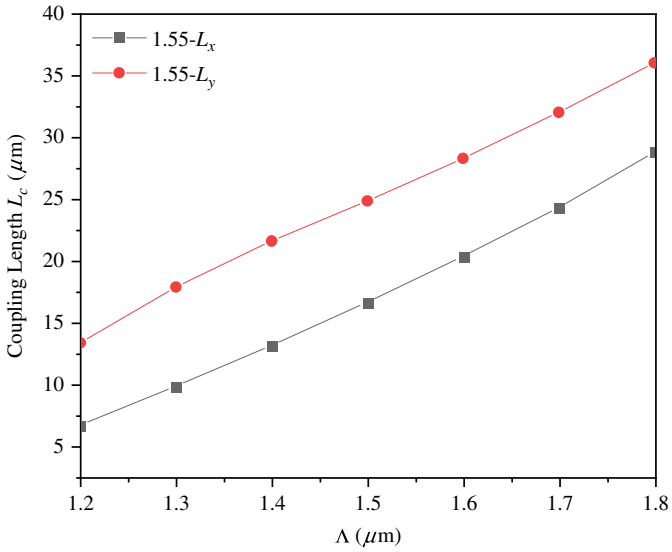

Fig. 3 Influence of Λ on the coupling length.

Figure 6 shows the coupling lengths in the x-polarization and y-polarization directions and CLR for different apertures of d_2. The coupling length in the y-polarization direction is greater than that in the x-polarization direction. As the aperture increases, the coupling length increases and coupling between the two cores becomes difficult. The optimal d_2 value is 0.21 μm.

Based on the aforementioned analysis, the optimal parameters of the PCF polarization beam splitter are as follows: $\Lambda = 1.2$ μm, $d_0 = 0.251$ μm, $d_1 = 1.4$ μm, and $d_2 = 0.21$ μm. The variation of the coupling lengths with wavelength is shown in Fig. 7, and the coupling lengths in the x- and y-directions decrease with increasing wavelength. At a wavelength of 1550 nm, the coupling lengths in the x-polarization and y-polarization directions are 6.6695 and 13.3390 μm, respectively. Figure 8 shows the relationship between the normalized power and transmission distance at 1550 nm. For a coupling length ratio $R = L_x/L_y = 0.5$, the fiber length L is $2 \times L_x = 1 \times Ly = 13.3390$ μm and the transmission distance is 13.3390 μm. That is, the two beams can basically be separated completely.

Figure 9 shows the change of the ERs with wavelengths. The ER is less than -10 dB when the wavelength is 1.445 to 1.645 μm and the bandwidth is 200 nm. At a wavelength of 1.55 μm, the ER is the largest with the absolute value reaching 143.49 dB. To account for possible errors in

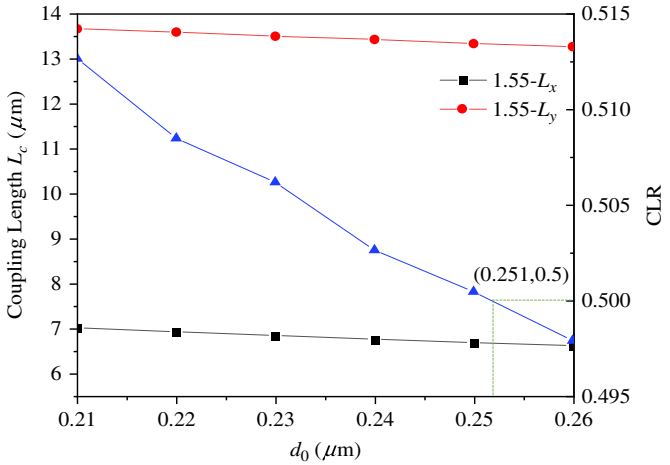

Fig. 4 Influence of d_0 on the coupling length and CLR.

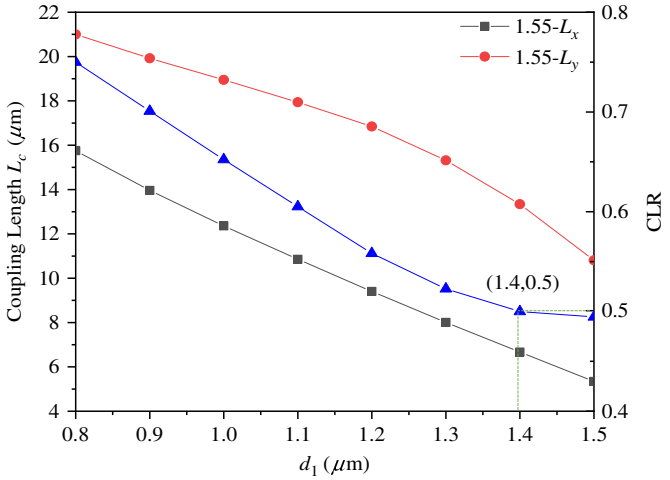

Fig. 5 Influence of d_1 on the coupling length and CLR.

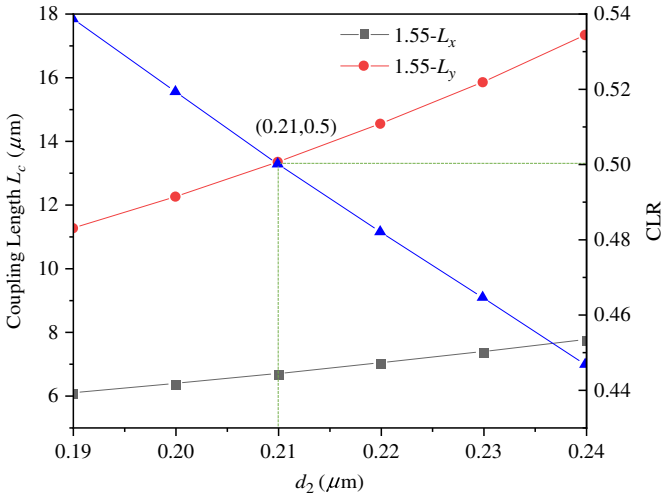

Fig. 6 Influence of d_2 on the coupling length and CLR.

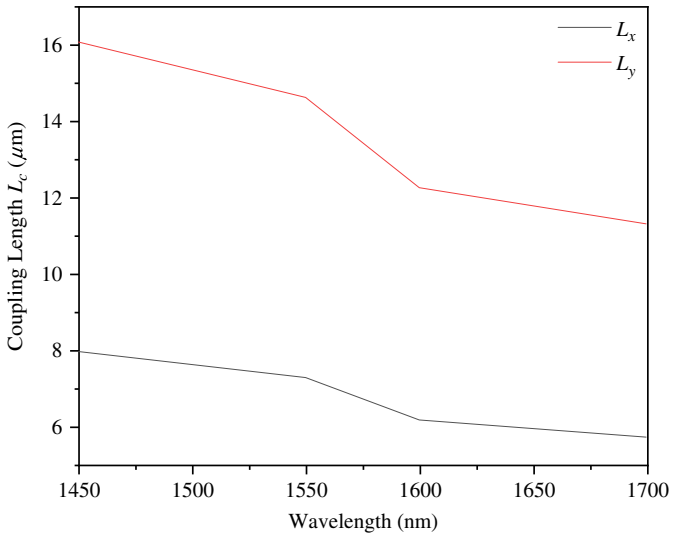

Fig. 7 Relationship between the coupling lengths of the polarization beam splitter and wavelength under optimal conditions.

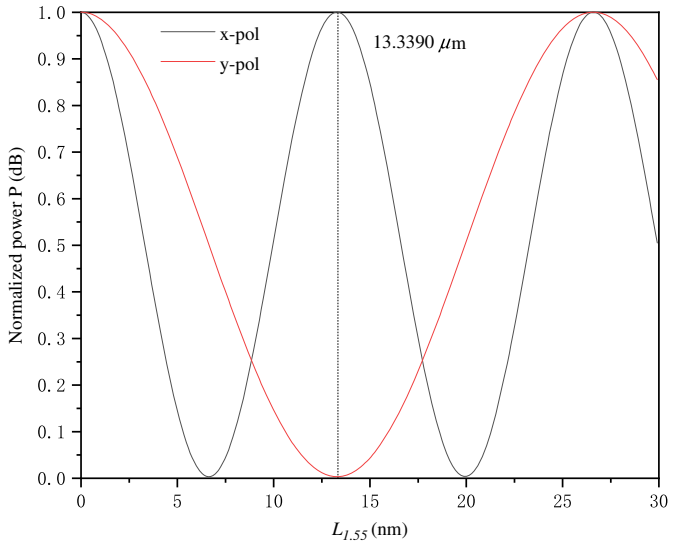

Fig. 8 Relationship between the normalized power and transmission distance at 1550 nm.

manufacturing, Fig. 10 shows the ER curve with a projected parameter error of $\pm 1\%$. An error of $\pm 1\%$ has almost no effects on the bandwidth, but the maximum ER is affected. All in all, because of the short length of the fiber, the influence of manufacturing errors is minimal.

Figure 11 shows the ER curves of the splitter at different temperatures (20°C, 25°C, and 30°C). By changing the temperature, there is almost no change in bandwidth or ER. Although wavelength and temperature are the two most important factors that affect the refractive index of NLC, the operating temperature can be controlled by a thermoelectric module. GaAs has higher electron mobility and saturation mobility, and it has a unique semi-insulating property. In addition, GaAs materials also have heat-resistant properties, and temperature has little effect on them, giving GaAs materials special uses and versatility; their applications have been extended to areas that silicon dioxide material devices cannot reach.

Table 1 compares the performance of this polarization beam splitter with those reported recently in the literature; the virtues of this polarization beam splitter, such as the small size, large ER, and broadband characteristics, are demonstrated.

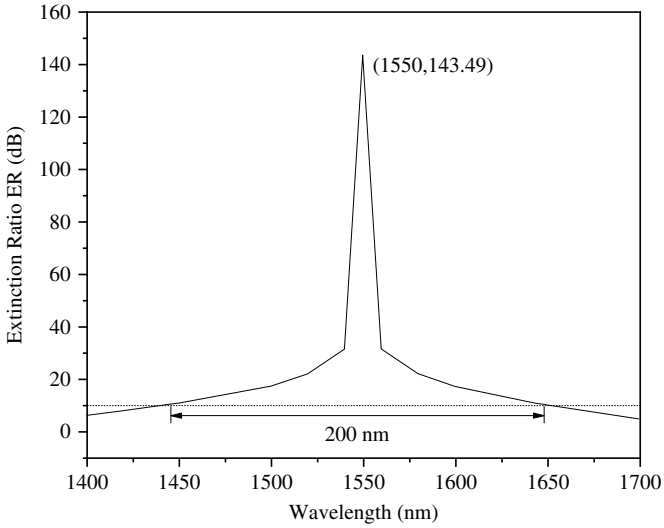

Fig. 9 Relationship between ERs and wavelengths.

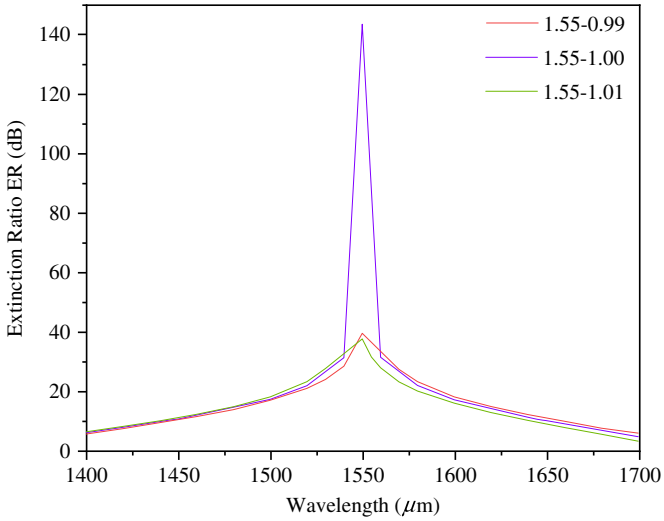

Fig. 10 ER curves for parameter error within ±1%.

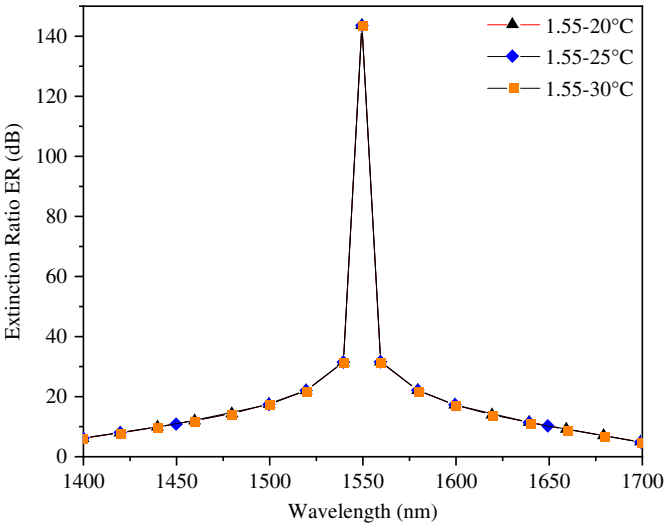

Fig. 11 Influence of different temperatures on ERs of beam splitters at 1550 nm.

Table 1 Comparison of the properties of the PCF polarization splitter described in this paper with those in the literature.

References	Length of the beam splitter (μm)	ER (dB)	Bandwidth (nm)
3	732.2	32	15.6
2	401	110.1	140
1	249	−50.7	17
27	89.05	107.21	150
28	47.26	−151.43	104
Our work	13.3390	143.49	200

4 Conclusion

A dual-core fiber-filled polarization beam splitter comprising NLC is designed, and the influence of various structural parameters on the coupling characteristics is studied analytically. By changing the diameter of the central and adjacent air holes, a polarizing beam splitter with a short length, ER, and wide bandwidth is obtained. The polarization beam splitter with a length of 13.3390 μm shows a bandwidth of 200 nm with an ER larger than 10 dB, and the largest ER is observed to be 143.49 dB. The performance of the simple and easy-to-manufacture polarization beam splitter is superior to that of similar splitters reported recently in the literature. Further, our results provide the theoretical background to facilitate the design of high-performance crystal fiber polarization beam splitters.

Acknowledgments

This work was jointly supported by the City University of Hong Kong Strategic Research Grant (Grant Nos. 7005105 and 7005265), Scientific Research Fund of Sichuan Province Science and Technology Department (Grant No. 2020YJ0137), and Local Universities Reformation and Development Personnel Training Supporting Project from Central Authorities (Grant No. 140119001).

References

1. J. Zi et al., "Short-length polarization splitter based on dual-core photonic crystal fiber with hexagonal lattice," *Opt. Commun.* **363**, 80–84 (2016).
2. Z. Xu et al., "Design of short polarization splitter based on dual-core photonic crystal fiber with ultra-high extinction ratio," *Opt. Commun.* **354**, 314–320 (2015).
3. Q. Xu et al., "A novel polarization splitter based on dual-core photonic crystal fibers," *Optik* **127**, 10442–10449 (2016).
4. X. Li et al., "Computationally efficient coherent detection and parameter estimation algorithm for maneuvering target," *Signal Process.* **155**, 130–142 (2019).
5. W. J. Tomlinson and C. Lin, "Optical wavelength-division multiplexer for the $1-1.4$ μm spectral region," *Electron. Lett.* **14**(11), 345–347 (1978).
6. J. R. Xue et al., "Polarization filter characters of the gold-coated and the liquid filled photonic crystal fiber based on surface plasmon resonance," *Opt. Express* **21**(11), 13733–13740 (2013).
7. Y. Liu et al., "Design of a single-polarization filter based on photonic crystal fiber with gold film on the inner wall of two ultra-large holes," *Opt. Laser Technol.* **114**, 114–121 (2019).
8. T. A. Birks, J. C. Knight, and P. S. J. Russell, "Endlessly single-mode photonic crystal fiber," *Opt. Lett.* **22**(13), 961–963 (1997).

9. Z. Ke, G. Chang-Ying, and L. I. Ai-Ping, "Supercontinuum generation in the photonic crystal fiber," *Opt. Commun. Technol.* **33**(10), 31–34 (2009).
10. K. Suzuki et al, "Optical properties of a low-loss polarization-maintaining photonic crystal fiber," *Opt. Express* **9**(13), 676–80 (2001).
11. L. Zhang and C. Yang, "Polarization splitter based on photonic crystal fibers," *Opt. Express* **11**(9), 1015–1020 (2003).
12. M. Yong et al., "A novel polarization splitter based on octagonal dual-core photonic crystal fiber," *Optoelectron. Lett.* **4**, 257–260 (2016).
13. M. Fahmi et al., "Twin-core sunflower-type photonic quasicrystal fibers incorporated gold, silver, and copper microwire: an ultrashort and broad bandwidth polarization splitter," *Opt. Quantum Electron.* **51**(5), 164 (2019).
14. J. E. Úsuga-Restrepo et al., "All-fiber circular polarization beam splitter based on helically twisted twin-core photonic crystal fiber coupler," *Opt. Fiber Technol.* **58**, 102285 (2020).
15. S. Selleri et al., "Complex FEM modal solver of optical waveguides with PML boundary conditions," *Opt. Quantum Electron.* **33**(4), 359–371 (2001).
16. K. R. Khan and T. Wu, "Finite element modeling of dual core photonic crystal fiber," *ACES J.* **23**(3), 215–219 (2008).
17. K. Saitoh and M. Koshiba, "Numerical modeling of photonic crystal fibers," *J. Lightwave Technol.* **23**(11), 3580–3590 (2005).
18. K. Khan, S. Bydnik, and T. Hall, "Tunable all optical switch implemented in a liquid crystal filled dual-core photonic crystal fiber," *J. PIERM* **22**, 179–189 (2012).
19. M. F. O. Hameed, S. S. A. Obayya, and R. J. Wiltshire, "Multiplexer–demultiplexer based on nematic liquid crystal photonic crystal fiber coupler," *Opt. Quantum Electron.* **41**(4), 315–326 (2009).
20. J. Li et al., "Infrared refractive indices of liquid crystals," *J. Appl. Phys.* **97**(7), 073501 (2005).
21. J. Li and S. T. Wu, "Extended Cauchy equations for the refractive indices of liquid crystals," *J. Appl. Phys.* **95**, 896 (2004).
22. Z. Wang et al., "Coupling in dual-core photonic bandgap fibers: theory and experiment," *Opt. Express* **15**(8), 4795–4803 (2007).
23. E. K. Akowuah et al., "Numerical analysis of a photonic crystal fiber for biosensing applications," *IEEE J. Quantum Electron.* **48**(11), 1403–1410 (2012).
24. J. N. Dash and R. Jha, "On the performance of graphene-based D-shaped photonic crystal fibre biosensor using surface plasmon resonance," *Plasmonics* **10**(5), 1123–1131 (2015).
25. N. Florous, K. Saitoh, and M. Koshiba, "Synthesis of polarization-independent splitters based on highly birefringent dual-core photonic crystal fiber platforms," *IEEE Photonics Technol. Lett.* **18**(11), 1231–1233 (2006).
26. W. Lu, S. Lou, and X. Wang, "Ultrabroadband polarization splitter based on three-core photonic crystal fibers," *Appl. Opt.* **52**(35), 8494–8500 (2013).
27. F. T. He et al., "Polarization splitter based on dual-core photonic crystal fiber with tellurite glass," *Optik* **164**, 624–631 (2018).
28. J. Lou, T. Cheng, and S. Li, "Ultra-short polarization beam splitter with square lattice and gold film based on dual-core photonic crystal fiber," *Optik* **179**, 128–134 (2019).

Sinuo An is a graduate student at Northeast Petroleum University.

Biographies of the other authors are not available.